JOURNAL OF THERMOPHYSICS AND HEAT TRANSFER
Vol. 22, No. 4, October–December 2008

Mathematical Modeling of Impinging Hydrogen–Air Flows Augmented by Catalytic Surface Reactions

Timothy W. Tong,* Mohsen M. Abou-Ellail,† and Yuan Li‡
George Washington University, Washington, D.C. 20052

DOI: 10.2514/1.34538

The catalytic combustion of hydrogen–air mixtures involves the adsorption of the fuel and oxidant into a platinum surface, chemical reactions of the adsorbed species, and the desorption of the resulting products. Readsorption of some produced gases is also possible. The catalytic reactions can be beneficial in porous burners that use low equivalence ratios. In this case, the porous burner flame can be stabilized at low temperatures to prevent any substantial gas emissions, such as nitrogen oxides. The present paper is concerned with the numerical computation of heat transfer and chemical reactions in hydrogen–air mixtures that impinge perpendicularly on a platinum-coated hot plate. Chemical reactions are included in the gas phase as well as in the platinum layer. In the gas phase, eight species are involved in 24 elementary reactions. On the platinum hot surface, additional surface species are included that are involved in 14 additional surface chemical reactions. The platinum surface temperature is fixed, whereas the properties of the reacting flow are computed. The flow configuration investigated in the present paper is that of impinging jets. Finite volume equations are obtained by formal integration over control volumes surrounding each grid node. Upwind differencing is used to ensure that the influence coefficients are always positive to reflect the real effect of neighboring nodes on a typical central node. The finite volume equations are solved iteratively for the reacting gas flow properties. On the platinum surface, surface species balance equations, under steady-state conditions, are solved numerically. A nonuniform computational grid is used, concentrating most of the nodes near the catalytic surface. The computed heat transfer numerical results are compared with the empirical data of similar geometry. A surface temperature of 1150 K caused fast reactions on the catalytic surface and in the flowing gas for some species, such as OH, HO_2, and H_2O_2. The computational results for heat transfer, mass transfer, and surface reaction rate at the gas–surface interface are correlated by nondimensional relations. These relations can be used as a submodel for the more complicated catalytic reactors.

Nomenclature

a_n = finite difference coefficients due to combined convection and diffusion
C_p = constant-pressure specific heat
h_g = gas sensible enthalpy
K_s = total number of elementary surface reactions
k_{fj} = forward kinetic rate constants of reaction j
M = molecular weight
Nu = Nusselt number
N_g = number of gas-phase species
N_s = number of surface species
P = gas pressure
R = universal gas constant
Re = Reynolds number
Sh = Sherwood number
$\dot{s}_k$ = surface production or depletion rate of the surface species k, $\mathrm{mole/cm^2/s}$
T_g = gas temperature
T_s = catalytic surface temperature
U = gas velocity along jet axis
U_{in} = jet inlet velocity
u_i = velocity in direction i
W_j = reaction rate of reaction j
$[X_k]$ = generalized concentration of species k (gas phase: $\mathrm{mole/cm^3}$, surface phase: $\mathrm{mole/cm^2}$)
x = distance along the axial axis
x_i = distance along direction i
Y = species mass fraction
Z = surface site concentration
z_k = surface site fraction of species k (surface coverage fraction)
Γ_h = thermal diffusivity
γ = sticking coefficient
δ = reaction boundary-layer thickness
μ = dynamic viscosity
ν_{lj} = stoichiometric coefficient of species l in reaction j
ρ = gas density

I. Introduction

CATALYSTS have been widely used in many industrial applications to control the process of chemical reaction. One of the applications of catalysts is catalytic combustion. With the assistance of catalysts, the ignition temperature of fuel is lower than the ignition temperature of the fuel without catalysts. Platinum and palladium are common catalysts used to assist combustion. Cattolica and Schefer [1,2] experimentally investigated the combustion of hydrogen–air mixtures in boundary-layer flows over catalytic and noncatalytic surfaces. Later, the kinetics of OH and H_2O formation on platinum was investigated experimentally by Ljungström et al. [3]. In their work, a hydrogen–air mixture was impinged on a platinum surface. Their experimental results were obtained at different inlet fuel concentrations, total pressures, and total temperatures. Their results showed that, at surface temperatures in the range of 900–1300 K, the water production was high and was determined mainly by the surface sticking coefficients. The combustion of several fuels, that is, NH_3, CH_4, C_3H_8, and a NH_3–CH_4 mixture, on a platinum surface in a stagnation flowfield

Presented as Paper 4624 at the 39th AIAA Thermophysics Conference, Miami, FL, 25–28 June 2007; received 11 September 2007; revision received 31 May 2008; accepted for publication 4 June 2008.

*Dean, School of Engineering and Applied Science, 725 23rd Street, Northwest. Associate Fellow AIAA.
†Visiting Professor, School of Engineering and Applied Science, 725 23rd Street, Northwest. Member AIAA.
‡Graduate Research Assistant, School of Engineering and Applied Science, 725 23rd Street, Northwest.

has been studied experimentally by Williams et al. [4]. In addition, the combustion of methane on a platinum surface has been studied numerically by Song et al. [5]. In [5], the surface reaction of methane over platinum has been modeled by a global reaction mechanism. Similarly, the combustion of hydrogen on a platinum surface in a stagnation flowfield and boundary-layer flowfield has been studied numerically by Warnatz et al. [6]. In their work, the elementary reaction mechanism of the oxidation of hydrogen on a platinum surface was introduced. It includes the absorption/desorption of reactants and products as well as the recombination reactions of the surface radicals. Warnatz et al. [6] also compared the computed [OH] concentration with experimental data from Cattolica and Schefer [1,2]. Thermochemical data of surface species involved in the surface reactions have also been published in [6]. Later, the elementary surface reaction mechanism of methane with platinum was established by Deutschmann et al. [7]. The detailed surface reaction mechanism has been used by Deutschmann et al. [7] to numerically simulate the experiments of Williams et al. [4] on the surface combustion of methane over platinum. It was found in [7] that methane is ignited at a surface temperature around 1000 K, and the reaction is fast between surface temperatures of 1000 and 1300 K; for surface temperatures below 1000 K, the surface reaction is slow and methane could not be ignited. Surface coverage of surface species and mole fractions of gas-phase species have been calculated in [7]. Raja et al. [8] used the detailed surface mechanisms for methane combustion developed by Deutschmann et al. [7] to model the catalytic honeycomb monolith combustion.

In the present paper, the catalytic combustion of impinging hydrogen–air mixtures is modeled numerically. The flow configuration is shown in Fig. 1. A unity equivalence ratio is used for the hydrogen–air mixtures, which impinge vertically over a flat hot plate. The jet exit section width is 3 cm. The surface of the flat plate is coated with platinum. The surface temperature of the flat plate is kept uniform, constant, and high enough to initiate catalytic combustion of the fuel–air mixture. The fuel and oxygen are consumed while products are generated at the hot catalytic surface through surface reactions. The present two-dimensional model of impinging jet flow, with surface reactions, is similar to the model developed by Tong et al. [9]. A multistep reaction mechanism is adopted for hydrogen–air gas-phase reactions. It involves 24 elementary reactions and 8 chemical species for hydrogen–air mixtures. The surface reaction mechanism developed by Deutschmann et al. [7] is adopted in the present work. This surface reaction mechanism for hydrogen–air mixtures consists of 14 elementary surface reactions and involves 4 gas-phase species and 5 surface species. The surface reaction model developed by Coltrin et al. [10] is also invoked in the present work. Nondimensional relations are developed to represent the mass transfer and reaction rates at the gas–surface interface.

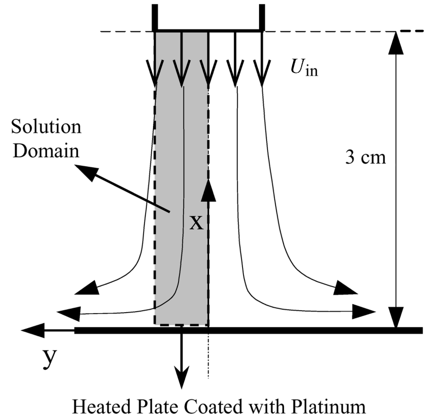

Fig. 1 Layout of impinging flow with surface reactions.

II. Mathematical Model and Solution Procedure

The numerical models for laminar flow, heat transfer, gas-phase combustion, and catalytic surface reactions are presented in this section. The flow configuration is shown in Fig. 1. The model can be classified into four main groups of equations as follows.

A. Continuity and Momentum Equations

The mass continuity of reacting flows may be written as

$$\frac{\partial(\rho)}{\partial t} + \frac{\partial(\rho u_i)}{\partial x_i} = 0 \tag{1}$$

The momentum equation for the laminar reacting flow may be written in Cartesian tensor notations as [11]

$$\frac{\partial(\rho u_j)}{\partial t} + \frac{\partial}{\partial x_i}(\rho u_j u_i) - \frac{\partial}{\partial x_i}\left(\mu \frac{\partial u_j}{\partial x_i}\right) = -\frac{\partial(P)}{\partial x_j} + \frac{\partial}{\partial x_i}\left[\mu\left(\frac{\partial u_i}{\partial x_j} - \frac{2}{3}\frac{\partial u_k}{\partial x_k}\delta_{ij}\right)\right] \tag{2}$$

where u_j is the gas velocity along coordinate x_j. The impinging flow of Fig. 1 has a vertical axis of symmetry. The gravity force, which is pointing toward the negative x coordinate, is neglected in the present study, as can be seen from Eq. (2). However, if P represents hydrodynamic pressure, then the gravity force can be dropped out from the momentum equation to be replaced by a buoyancy force, which is also neglected in the present axially symmetric impinging vertical flow.

B. Energy Equations

The energy equation for the reacting flow is

$$\frac{\partial \rho h_g}{\partial t} + \frac{\partial}{\partial x_i}(\rho u_i h_g) - \frac{\partial}{\partial x_i}\left(\Gamma_h \frac{\partial h_g}{\partial x_i}\right) = -\sum_j (\Delta H_j) W_j \tag{3}$$

where ΔH_j and W_j are the enthalpy of the reaction and the reaction rate of the chemical reaction j of the reaction mechanism involving hydrogen–air mixtures (Table 1). In these equations, the subscript g denotes the gas phase. The gas temperature, T_g, at any point is directly related to the local gas sensible enthalpy, h_g; the gas species mass fractions, Y_j; and the constant-pressure specific heats, namely,

$$h_g = \int \left(\sum_j C_{pj} Y_j\right) \mathrm{d}T \tag{4}$$

The lower limit of the integration is 298 K, whereas the upper limit equals T_g.

C. Species Mass Fraction Equations

The species mass fractions in reacting flows may be written as

$$\frac{\partial(\rho Y_l)}{\partial t} + \frac{\partial(\rho u_i Y_l)}{\partial x_i} - \frac{\partial}{\partial x_i}\left(\Gamma_{Y_l} \frac{\partial Y_l}{\partial x_i}\right) = M_l \sum_j \nu_{lj} W_j \tag{5a}$$

where Y_l is the mass fraction of species l, G_{Yl} is its molecular diffusivity, M_l is the molecular mass of species l, and ν_{lj} is the stoichiometric coefficient of species l in reaction j. The rates of production of the chemical species W_j in Eq. (3) may be written as

$$W_j = A_j T^{\alpha_j} \exp\left(-\frac{E_j}{RT_g}\right) \prod_{\kappa=1}^{N} \left(\frac{\rho Y_\kappa}{M_\kappa}\right)^{\upsilon'_{ij}} \tag{5b}$$

where A_j is the frequency factor, α_j is the preexponential temperature exponent, and E_j is the activation energy of reaction j, as given in Table 1. The reactants' stoichiometric coefficients are denoted by υ'_{ij}. The molecular weight of species k is denoted by M_k, whereas N is the number of reacting gas species involved. As shown in Table 1, the mechanism consists of 24 elementary reactions, which is a

Table 1 Gas-phase reaction mechanism

No.	Reaction	A_j, mole, cm^3, s	α_j	E_j, KJ/mole
lf	$O_2 + H \rightarrow OH + O$	2.000×10^{14}	0.00	70.30
lb	$OH + O \rightarrow O_2 + H$	1.568×10^{13}	0.00	3.52
2f	$H_2 + O \rightarrow OH + H$	5.060×10^{4}	2.67	26.3
2b	$OH + H \rightarrow H_2 + O$	2.222×10^{4}	2.67	18.29
3f	$H_2 + OH \rightarrow H_2O + H$	1.000×10^{8}	1.60	13.8
3b	$H_2O + H \rightarrow H_2 + OH$	4.312×10^{8}	1.60	76.46
4f	$OH + OH \rightarrow H_2O + O$	1.500×10^{9}	1.14	0.42
4b	$H_2O + O \rightarrow OH + OH$	1.473×10^{10}	1.14	71.09
5f	$O_2 + H + M \rightarrow HO_2 + M$	2.300×10^{18}	−0.80	0.00
5b	$HO_2 + M \rightarrow O_2 + H + M$	3.190×10^{18}	−0.80	195.39
6	$HO_2 + H \rightarrow OH + OH$	1.500×10^{14}	0.00	4.20
7	$HO_2 + H \rightarrow H_2 + O_2$	2.500×10^{13}	0.00	2.90
8	$HO_2 + OH \rightarrow H_2O + O_2$	6.000×10^{13}	0.00	0.00
9	$HO_2 + H \rightarrow H_2O + O$	3.000×10^{13}	0.00	7.20
10	$HO_2 + O \rightarrow OH + O_2$	1.800×10^{13}	0.00	−1.70
11	$HO_2 + HO_2 \rightarrow H_2O_2 + O_2$	2.500×10^{11}	0.00	−5.20
12f	$OH + OH + M \rightarrow H_2O_2 + M$	3.250×1022	−2.00	0.00
12b	$H_2O_2 + M \rightarrow OH + OH + M$	1.692×1024	−2.00	202.29
13	$H_2O_2 + H \rightarrow H_2O + OH$	1.000×1013	0.00	15.00
14f	$H_2O_2 + OH \rightarrow H_2O + HO_2$	5.400×1012	0.00	4.20
14b	$H_2O + HO_2 \rightarrow H_2O_2 + OH$	1.802×1013	0.00	134.75
15	$H + H + M \rightarrow H_2 + M$	1.800×1018	−1.00	0.00
16	$OH + H + M \rightarrow H_2O + M$	2.200×1022	−2.00	0.00
17	$O + O + M \rightarrow O_2 + M$	2.900×1017	−1.00	0.00

compromise between the full reaction and the skeletal reaction mechanisms. The chemical kinetic mechanism involves 8 species, namely, O_2, O, OH, H, H_2, H_2O, HO_2, and H_2O_2, whereas the 24 involved elementary reactions are discussed in detail by Tong et al. [12] and Peters [13,14]. It should be mentioned here that ν_{lj} is taken as a positive value for products and a negative value for reactants as required for the proper summation of the effect of each reaction on the production of a particular species. The thermodynamic data needed in the present computations can be found using CHEMKIN [15]. The gas physical properties are taken as temperature dependant. The density is computed from the ideal gas equation of state whereas the species constant-pressure specific heats and gas viscosities are computed from standard temperature polynomials. The remaining gas physical properties can then be obtained from the aforementioned physical properties, which are included in the Prandtl and Lewis numbers. In the present work, the gas Prandtl number is equal to 0.7 whereas a unity Lewis number is assumed. It should be mentioned here that most combustion products have a nearly unity Lewis number except for gases with lower molecular weights, such as H and H_2, which are rare species in hydrogen–air combustion products. Moreover, for forced convection flows, diffusion is of secondary importance.

D. Surface Reactions

For a steady-state problem, the solution has no change with respect to time. Thus, the surface coverage of any surface species with respect to time is zero. The variation of the surface coverage with respect to time can be computed from the net production of each surface species. The conservation of the surface coverage of species k may be written as [6]

$$\frac{\mathrm{d}z_k}{\mathrm{d}t} = \frac{\dot{s}_k}{Z} \tag{6}$$

where Z is the total surface site density and the surface density used in the present paper is 1.63×10^{15} cm^{-2} [7].

Because the present reacting flow includes gas–surface interactions, the mass transfer between the gas phase and the catalytic surface needs to be included when solving the species mass fractions of the flowing gas. The mass fluxes transferred through the convection and diffusion processes at the gas–surface interface of any gas-phase species are balanced by the production or depletion rates of that species by surface reactions. The surface boundary condition of each gas-phase species k based on the mass balance is given by Coltrin et al. [10] as

$$n \cdot [\rho Y_k (V_k + u)] = \dot{s}_k M_k \tag{7}$$

where n is the unit normal vector pointing outward to the surface and u is the bulk fluid velocity. The diffusion velocity is V_k.

The production rate of each species $\dot{s}_k$, either the gas-phase species or surface species, may be written as [16]

$$\dot{s}_k = \sum_{j=1}^{K_s} \nu_{k_j} k_{f_j} \prod_{k=1}^{N_g+N_s} [X_k]^{\nu'_{k_j}} \tag{8}$$

where ν'_{kj} is the left-hand side stoichiometric coefficients of the reaction equation, and ν_{kj} is the right-hand side minus the left-hand side stoichiometric coefficients of the reaction equation. The species concentration is $[X_k]$ and the units of gas-phase species and surface species concentrations are mole/cm^3 and mole/cm^2, respectively.

A detailed surface reaction mechanism is used to model the gas–surface interaction between the fuel and platinum. The surface reaction mechanism adopted in the present work for hydrogen–air mixtures reacting over platinum-coated surfaces is established by Deutschmann et al. [7]; it is shown in Table 2. Deutschmann et al. [7] analyzed the uncertainties in the surface reaction mechanism shown in Table 2 and rationalized the use of preexponential constants obtained either experimentally or through quantum-mechanical analytical studies. The surface chemical species are denoted by a label, s, as shown in Table 2. The surface reaction mechanism consists of 14 elementary reactions and involves four gas-phase species, namely, O_2, OH, H_2, and H_2O, and five surface species, namely, O(s), OH(s), H(s), H_2O(s), and Pt(s). The reaction rate constants are described in terms of either an Arrhenius expression or a sticking coefficient, γ. The Arrhenius expression form is

$$k_{fj} = A_j \exp\left(\frac{-E_j}{RT}\right) \tag{9}$$

The sticking coefficient can be converted to the usual kinetic rate constants via the relation given by Coltrin et al. [10]:

$$k_{fj} = \frac{\gamma}{1 - \gamma/2} \frac{1}{Z^m} \sqrt{\frac{RT_g}{2\pi M}} \tag{10}$$

where Z is the total surface site concentration, m is sum of the surface reactants' stoichiometric coefficient, and M is the molecular weight

Table 2 Surface reaction mechanism [7]

No.	Reaction	A_j; mole, cm^3, s	E_j, KJ/mole	Sticking coeff.
1	$H_2 + P_t(s) + P_t(s) \rightarrow H(s) + H(s)$	——	——	0.046
2	$H(s) + H(s) \rightarrow P_t(s) + P_t(s) + H_2$	1.0×10^{21}	67.4	——
3	$O_2 + P_t(s) + P_t(s) \rightarrow O(s) + O(s)$	——	——	0.023
4	$O(s) + O(s) \rightarrow P_t(s) + P_t(s) + O_2$	1.0×10^{21}	213.2	——
5	$H_2O + P_t(s) \rightarrow H_2O(s)$	——	——	0.75
6	$H_2O(s) \rightarrow H_2O + P_t(s)$	1.0×10^{13}	40.3	——
7	$OH + P_t(s) \rightarrow OH(s)$	——	——	1
8	$OH(s) \rightarrow OH + P_t(s)$	1.0×10^{13}	192.8	——
9, 10	$O(s) + H(s) \leftrightarrow OH(s) + P_t(s)$	1.0×10^{21}	11.5	——
11, 12	$H(s) + OH(s) \leftrightarrow H_2O(s) + P_t(s)$	1.0×10^{21}	17.4	——
13, 14	$OH(s) + OH(s) \leftrightarrow H_2O(s) + O(s))$	1.0×10^{21}	48.2	——

of the gas-phase species. The thermochemical data needed to determined the rate coefficients for the reverse reactions and enthalpies of the surface species are provided by Warnatz et al. [6].

E. Numerical Solution Procedure

The two-dimensional flow over the catalytic surface, shown in Fig. 1, is overlaid with a finite grid of nodes. At each nodal point, Eqs. (2), (3), and (5) and the pressure correction counterpart of Eq. (1) are formally integrated over a surrounding control volume. The faces of the control volume bisect the distances between that particular node and the four nearest neighbor nodes. The formal integration is performed with due care to preserve the physical meaning and overall balance of each dependent variable. The final form of the finite difference equations are written as follows [10]:

$$\left(\sum(a_n) - S_P\right)\Psi_P = \sum(a_n\Psi_n) + S_u \tag{11}$$

where Ψ stands for any of the dependent variables, namely, the axial and radial velocity components, gas sensible enthalpy, species mass fractions, and the pressure correction that is used to satisfy both the mass continuity and momentum equations simultaneously. The summation, $\sum$, is over the four neighbors, n, of a typical node, p. These finite difference coefficients, a_n, are computed using the upwind method, such that these coefficients are always nonnegative to give the proper combined effects of convection and diffusion. The coefficients of the integrated source term at node p are S_p and S_u.

The solution procedure is based on the line-by-line, alternating direction, tridiagonal matrix algorithm. This solution procedure is based on solving each line of nodes as a tridiagonal matrix and then sweeping the whole computational grid by sequentially solving the adjacent lines. Details of this algorithm are given by Abou-Ellail et al. [11]. The difference equations [Eq. (11)] for each dependant variable are modified at the boundaries of the solution domain, shown in Fig. 1, to impose the conditions there. The number of nodes along the x axis is 302, because most of the changes occur axially. However, only 10 transverse nodes can be used to cover the jet inlet section. On the flat plate surface, the velocity components vanish, whereas all the other dependent variables' normal gradients reflect the mass and heat fluxes due to surface reactions, as dictated by Eq. (7). Along the jet axis of symmetry, the normal gradient is equal to zero for all variables except the transverse velocity, which itself equals zero. At the outer jet boundary (i.e., at the outer boundary along the y coordinate), the gas is leaving the jet boundary along the positive side of the y coordinate. Therefore, the numerical values inside the solution domain are not affected by the values prevailing in the outgoing gases at the jet boundary. This type of boundary condition has usually been imposed as a zero-value normal gradient [11], as presumed in the present work. This is incorporated in the solution procedure as zero value for the coefficient connecting the last grid node along the y coordinate, inside the solution domain, and the boundary node of the outflowing gases along the outer jet boundary. It should be mentioned here that this finite difference coefficient is affected by the upwind scheme and hence assumes a zero value, automatically canceling the imposed known value boundary condition that may otherwise be assumed. Therefore, along the axial nodes adjoining the jet boundary, the normal gradients of all variables are equal to zero. At the inlet section, all variables are known from the specified incoming impinging jet conditions. Within each computational loop of the gas phase, Eq. (6) is solved iteratively for all surface species concentrations over the catalytic surface for the case of steady-state conditions, that is, $\mathrm{d}(z_k)/\mathrm{d}t = 0$. At the jet axis of symmetry, the transverse velocity is equal to zero. One thousand outer iterations were required for the complete conversion of the gas-phase equations of the main gaseous components. On the other hand, within each outer iteration, 200 inner iterations were necessary for the surface species to converge without any appreciable fluctuations. An additional 1000 iterations were performed to assure the conversion and stability of the intermediate and rare species, such as HO_2 and H_2O_2. The present numerical solution procedure has been validated by Tong et al. [17,18] for the combustion of methane–air mixtures on catalytic surfaces for impinging and boundary-layer flows. The use of the simplified one-dimensional model [7] is less accurate than its two-dimensional counterpart. The accuracy of the two-dimensional model is four times better than the one-dimensional model, as demonstrated by Tong et al. [9] through the computation of the elemental balance of carbon in the catalytic reactions of premixed methane–air impinging flows.

III. Presentation and Discussion of Results

The hydrogen–air mixture flow of uniform velocity impinges onto a hot flat plate coated by platinum at an angle of 90 deg. The impinging jet exit section is 3 cm from the catalytic surface, as depicted in Fig. 1. In addition to an inlet velocity of 15 cm/s, inlet velocities of 5, 30, 60, 100, 150, and 200 cm/s are used in the present computations to study the influence of inlet velocity on surface reactions. The computed Reynolds numbers, corresponding to the aforementioned inlet velocities, range from 58 to 2315. The momentum, heat, and mass transfer of the impinging flowfield as well as the catalytic reactions at the surface are computed for each inlet velocity. In the present numerical simulations, the equivalence ratio of the hydrogen–air mixture at the inlet is equal to 1.0 and the inlet temperature of the gas mixture is 300 K. The flat plate surface temperature is fixed at 1150 K in the present simulations. However, other surface temperatures are also considered, namely, 1000 and 1300 K. The modeling of the extinction process is not included in the present work. However, the interest is focused on the effect of the surface temperature on the catalytic-surface reactions and their effect on the gas-phase reactions in impinging jets. The surface temperature can be fixed by the electric heating or the cooling of the catalytic surface to obtain a particular temperature. The electric heating was considered by Deutschmann et al. [7] to obtain a fixed surface temperature. The computational results, which include heat transfer, mass transfer, surface reaction rate, the surface species coverage, the mole fractions of gas-phase species, and temperature profiles, are presented in this section.

A. Catalytic Surface Numerical Results

The Sherwood number, Sh, is used as a representative of the mass transfer of species between the reacting gas phase and the platinum surface species that take part in the heterogeneous reactions. The Sherwood number of the major species, O_2, H_2, and H_2O, is computed at different Reynolds numbers. To investigate different flow conditions, Sherwood numbers are obtained for two different surface temperatures. The Sherwood numbers of O_2, H_2, and H_2O are plotted vs the Reynolds number at surface temperatures of 1150 and 1000 K, as shown in Fig. 2. The numerical results show that, at a fixed value of Reynolds number, the difference among the values of the major species' Sherwood numbers is small enough to allow a unique equation for the Sherwood number vs the Reynolds number. Thus, at a fixed Reynolds number, the value of Sh of all the major species can fairly be represented by one mean value. With this approximation, the relation between the Sh of major species and the Re can be correlated into a single exponential function using curve fitting methods. For the impinging flow configuration, the relation between the Sh and the Re is correlated as

$$Sh = 0.65 + 0.0031 Re^{1.11}, \qquad T_s = 1150 \text{ K} \tag{12a}$$

$$Sh = 0.62 + 0.0029 Re^{1.01}, \qquad T_s = 1000 \text{ K} \tag{12b}$$

This correlation is also plotted in Fig. 2. It can be concluded from Fig. 2 that, for surface temperatures of 1150 and 1000 K, the mass transfer coefficient between the impinging gas main species and the surface species increases with increasing values of the inlet Reynolds number. The effect of the Reynolds number on the Sherwood number is attributed to the reduction in the thickness of the boundary layer and, hence, the increase in the mass transfer rate with increasing values of Reynolds number. The difference between the constants of Eqs. (12a) and (12b) varies between 5 to 10%. The Sherwood number is somewhat higher at higher surface temperatures for a fixed value of the inlet Reynolds number. Similarly, the surface reaction rates of the major species at a fixed value of Reynolds number can also be approximated by a mean value. The relation between the surface reaction rate, in $\text{mole}/\text{cm}^2/\text{s}$, and the Reynolds number for a surface temperature of 1150 K is correlated as

$$\text{reaction rate} = 9 \times 10^{-7} + 3.81 \times 10^{-9} Re^{1.12} \tag{13}$$

The computed values of the reaction rates and the curve fitting function of the reaction rate are plotted in Fig. 3. It can be seen from Fig. 3 that surface reactions are more active at higher inlet velocities. The correlations in Eqs. (12) and (13) show that both the Sherwood number and the rate of the surface reaction increase almost linearly with the Reynolds number. Equation (13) implies that, at 1150 K and a unity equivalence ratio, hydrogen–air mixtures react on catalytic surfaces as a one-step global reaction, given as $H_2 + 1/2O_2 \rightarrow H_2O$, with a reaction rate computed from the aforementioned correlation. Needless to say, the constants of Eq. (13) are dependant on the surface temperature and the equivalence ratio. Equations (12) and (13) have the same general characteristics as their counterparts, which were obtained by Tong et al. [9] for the catalytic combustion of impinging methane–air flows. However, the present surface reaction rate for hydrogen–air mixtures is nearly double that of its methane–air counterpart.

Figure 4 shows the surface coverage of different surface species vs Reynolds number. The surface coverage of O(s), H(s), H_2O(s), and OH(s) are depicted in log scale to show their discrete magnitudes. However, the surface coverage of Pt(s) is plotted, conveniently, in Fig. 4 along a linear ordinate. Figure 4 shows that, when the hydrogen is ignited and the surface reactions reach steady state, most of the catalytic surface is covered with active platinum sites for all

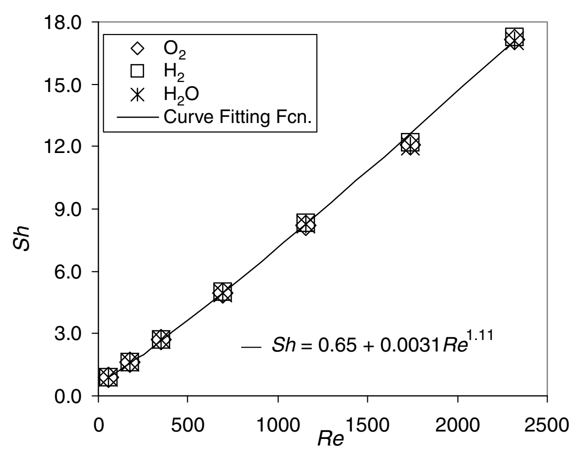

a) T_s = 1150 K

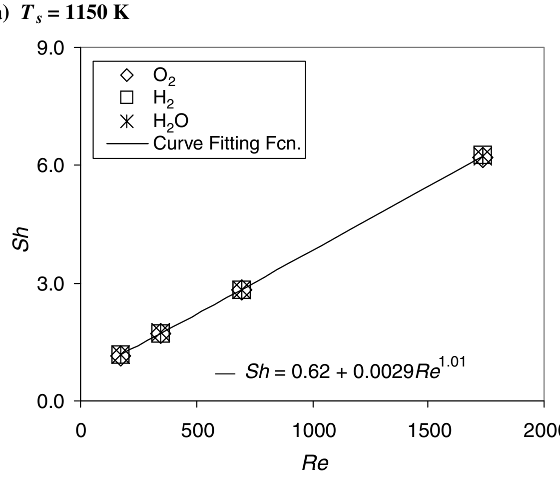

b) T_s = 1000 K

Fig. 2 Sherwood number vs Reynolds number.

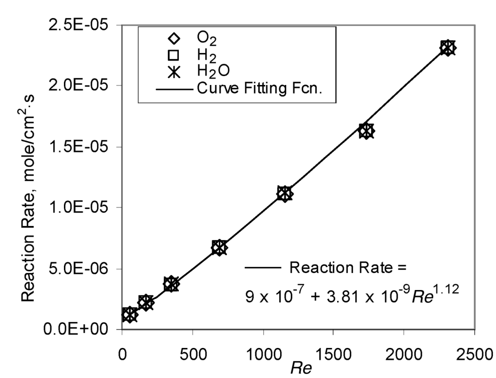

Fig. 3 Reaction rate vs Reynolds number.

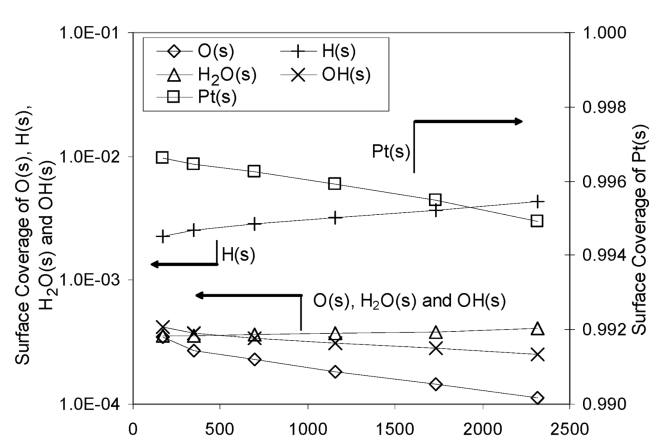

Fig. 4 Surface coverage at difference inlet velocities.

Reynolds numbers. The surface coverage of other surface species is small. The Pt(s) has the highest surface coverage, whereas O(s) has the lowest surface coverage. This is an outcome of a highly active catalytic surface at 1150 K.

B. Gas-Phase Numerical Results

Figures 5 and 6 show species mole fractions vs the distances above the surface along the jet axis of symmetry at an inlet velocity of 15 cm/s. Figure 5 shows the mole fraction profiles of O_2 and H_2. As shown in Fig. 5, for an equivalence ratio of 1.0, the oxygen and hydrogen are completely consumed at the catalytic surface. The mole fraction profile of the major combustion product, H_2O, is shown in Fig. 6.

The temperature profile along the jet centerline is depicted in Fig. 7. Temperature changes are confined to a distance of less than 0.8 cm above the catalytic surface. Although some gas-phase reactions are active near the hot surface, these reactions have slight effect on the local gas temperature, as can be seen from Fig. 7.

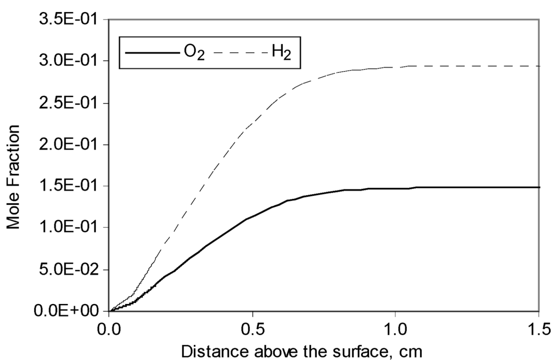

Fig. 5 Mole fractions of O_2 and H_2 above the surface at 1150 K and $U_{in} = 15$ cm/s.

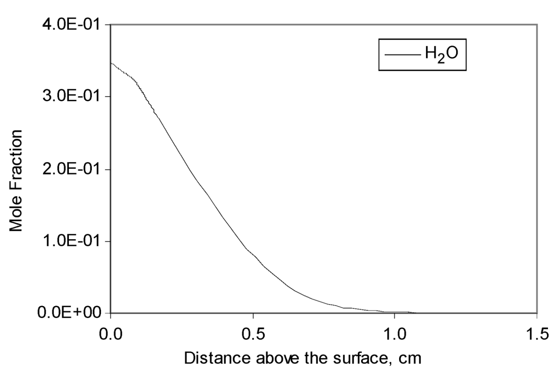

Fig. 6 Mole fractions of H_2O above the surface at 1150 K and $U_{in} = 15$ cm/s.

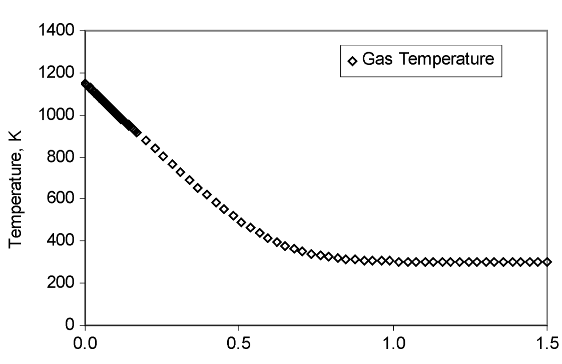

Fig. 7 Temperature profile above the surface at 1150 K and $U_{in} = 15$ cm/s.

Figures 8 and 9 depict the axial profiles of the rare species produced by the combined effect of the heterogeneous surface and gas-phase reactions. Most of these species are produced by the gas-phase reactions and, hence, these peaks have shifted from the catalytic surface. Moreover, the O atom is consumed on the catalytic surface, whereas the H atom and OH radical are produced on the surface, as depicted in Fig. 8. Figure 9 shows that H_2O_2 and HO_2 are produced in the sublayer near the catalytic surface for $x < 0.1$ cm. Most of the production of these unstable species is endothermic in nature. The grid used in the present paper is the one that produced grid-independent solutions. This numerical grid converges toward the catalytic surface. For this grid, more than 200 nodes occupy the thin sublayer with a thickness of 0.7 cm causing the grid nodes, in some figures, to fall on top of each other. Finer grids were not able to produce better numerical results for the data of Figs. 8 and 9 that describe the extremely small values of the rare species, which range between 10^{-7} and 10^{-10}.

Reactants and product mole fractions and dimensionless jet-centerline velocity profiles for two values of inlet velocity, namely, $U_{in} = 15$ and 150 cm/s, are shown in Fig. 10. The corresponding temperature profiles are depicted in Fig. 11. As the inlet jet velocity increases, the boundary layer is being squashed on the surface. This is an outcome of the upwind convection of the incoming gas mixture. However, the resulting shorter boundary layer can still consume the incoming hydrogen as a consequence of the increased surface reaction rates imposed by the present new correlation of Eq. (13). At $U_{in} = 15$ cm/s, the gas-phase mole fractions' variations are limited to a distance of 1.0 cm above the catalytic surface. However, for $U_{in} = 150$ cm/s, the active boundary layer is squeezed into a distance of 0.25 cm above the catalytic surface, as can be seen in Fig. 10. Similarly, the product mole fractions and temperature profiles, depicted in Fig. 11, indicate that, as the inlet velocity increases from 15 to 150 cm/s, the active boundary-layer thickness decreases from 1.0 to 0.25 cm above the catalytic surface. This behavior of the boundary layer is consistent with the previous findings of Tong et al. [9].

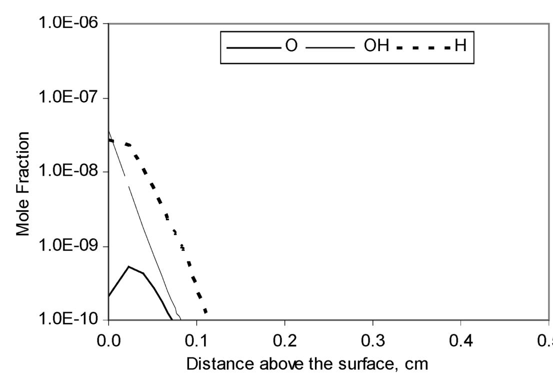

Fig. 8 Mole fractions of O, OH, and H above the surface at 1150 K and $U_{in} = 15$ cm/s.

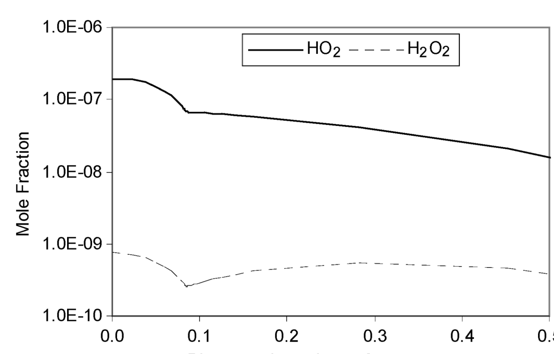

Fig. 9 Mole fractions of HO_2 and H_2O_2 above the surface at 1150 K and $U_{in} = 15$ cm/s.

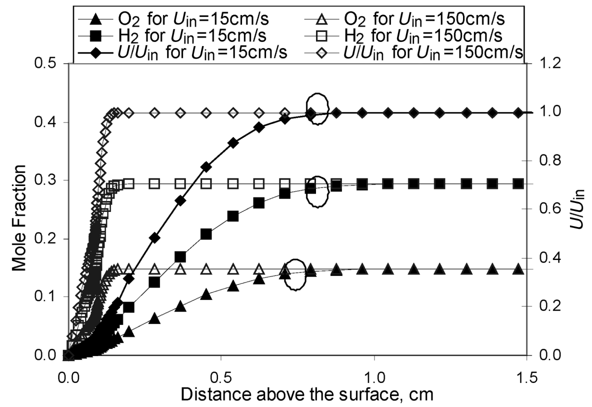

Fig. 10 Reactants' mole fractions and velocity profiles for U_{in} = 15 cm/s and U_{in} = 150 cm/s.

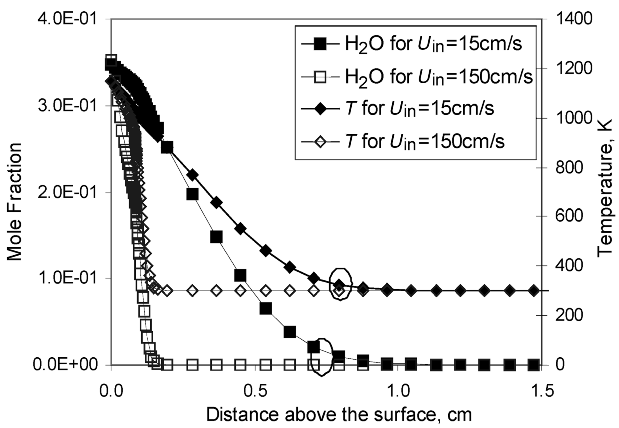

Fig. 11 Product mole fractions and temperature profiles for U_{in} = 15 cm/s and U_{in} = 150 cm/s.

C. Heat Transfer Numerical Results

The numerical results for different Reynolds numbers can be used to compute the heat transfer coefficient at the surface. This is done by computing the surface heat flux from the temperature gradient at the catalytic surface. Figure 12 shows the variation of the stagnation Nusselt number, Nu, vs Reynolds number, Re. Both the Nu and the Re are based on the jet width and inlet gas physical properties. It can be seen that the Nusselt number increases as the Reynolds number increases. This is attributed to the decrease in the active boundary-layer thickness as the Reynolds number increases. The shrinking of the active boundary layer causes the temperature gradient near the catalytic surface to increase as the Reynolds number increases, as can be seen in Fig. 11.

The heat transfer correlation for the stagnation point computed from the numerical data is

$$Nu = 0.69Re^{0.54} \tag{14}$$

For air with $Pr = 0.7$, the heat transfer correlation for the stagnation point is given by Beitelmal et al. [19] as:

$$Nu = CRe^{0.5} \tag{15}$$

where the value of constant C is given for the impinging air jet by Beitelmal et al. [19] as 0.824. The correlations (14) and (15) are valid for a unity jet height from surface to width ratio. The present correlation is in good agreement with the empirical Nusselt relation for impinging jets. However, the present results for reacting impinging jets predicts a slightly higher dependence of the Nu on the Re. This effect could be attributed mainly to species exchange at the catalytic surface, which may affect the gas mixture constant-pressure specific heat and density.

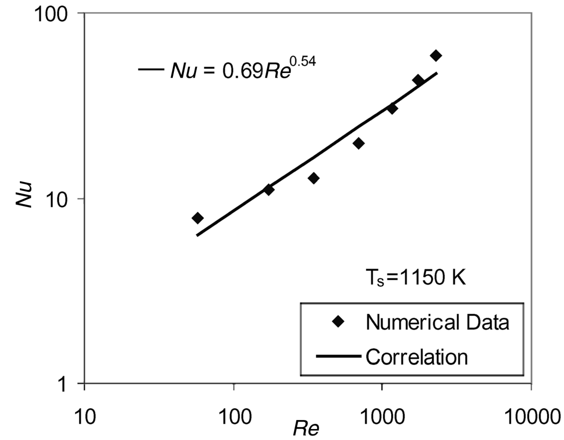

Fig. 12 Heat transfer correlations.

D. Surface Chemical Kinetics Numerical Results

The surface production rates, presented in Fig. 3 for a surface temperature of 1150 K, suggest that a global one-step reaction between O_2 and H_2 to produce H_2O is possible. Therefore, the following catalytic surface chemical reaction is considered:

$$H_2 + 1/2O_2 \rightarrow H_2O \tag{16}$$

Although (16) is not an elementary reaction, it is possible to represent its reaction rate with the following chemical kinetic equation:

$$R_c = A([O_2][H_2])^n \exp(-(T_a/T_s)) \tag{17}$$

where T_a and T_s are the activation and catalytic surface temperatures. The concentrations of the oxygen and hydrogen have units of mole/cm^3, whereas the surface reaction rate R_c is in mole/(cm$^2\cdot$s). This equation can presumably be used for a range of surface temperatures in the vicinity of 1150 K. The constants A, n, and T_a are to be computed from the present numerical data. To establish the relation between the surface reaction rate and the product of the concentrations of O_2 and H_2, the surface reaction rate, R_c, is plotted vs $[O_2][H_2]$ in Fig. 13 for $T_s = 1000$ K, in Fig. 14 for $T_s = 1150$ K, and in Fig. 15 for $T_s = 1300$ K. It should be mentioned here that the concentrations involved in Figs. 13–15 are computed at the gas–surface interface, that is, at $x = 0$. It was necessary to perform additional simulation runs for surface temperatures of 1000 and 1300 K to compute and validate the numerical values of the constants A, n, and T_a. The values of these constants are shown explicitly in the following surface reaction rate equation, namely,

$$R_c = 2.956 \times 10^7([O_2][H_2])^{0.661} \exp(-(5512/T_s)) \tag{18}$$

Equation (18) would be very useful in simplifying the computations of reacting hydrogen–air mixtures that impinge

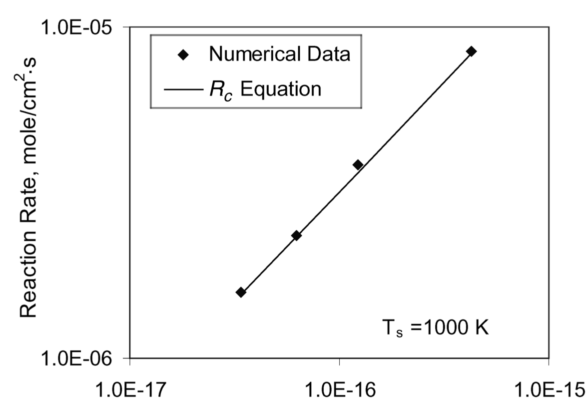

Fig. 13 Surface reaction rate at a surface temperature of 1000 K.

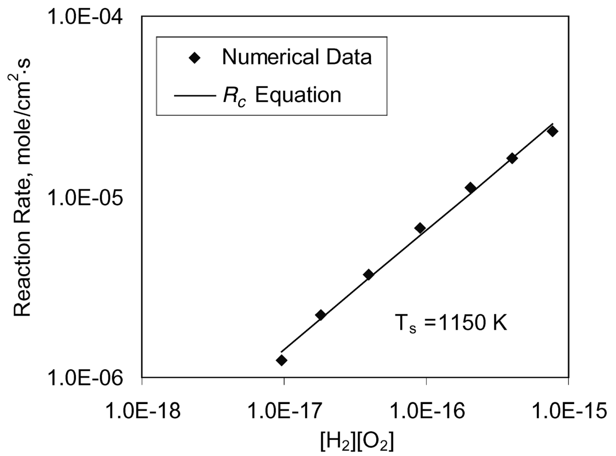

Fig. 14 Surface reaction rate at a surface temperature of 1150 K.

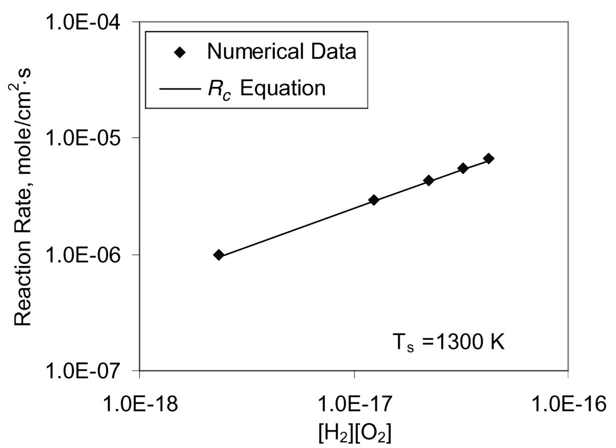

Fig. 15 Surface reaction rate at a surface temperature of 1300 K.

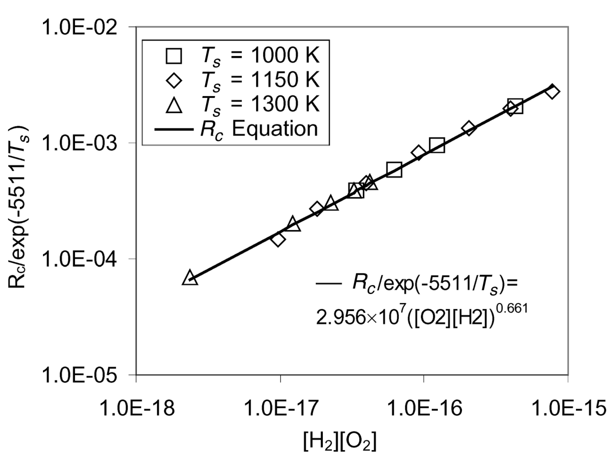

Fig. 16 $R_c/(\exp(-5511/T_s)$ vs $[H_2][O_2]$ for 1000, 1150, and 1300 K surface temperatures.

catalytic surfaces. Figure 16 depicts $R_c/(\exp(-5511/T_s)$ vs $[H_2][O_2]$ for surface temperatures of 1000, 1150, and 1300 K. The solid line in Fig. 16 represents the values computed directly from Eq. (18), whereas the present numerical results are plotted as separate data points at surface temperatures of 1000, 1150, and 1300 K. The data of Fig. 16 are in mole · cm · K units. Figure 16 shows clearly that the numerical data points are in good agreement with Eq. (18). The aforementioned result shows that Eq. (18) can be used to bypass the time consuming solutions of surface reactions that involve chemical kinetics similar to those indicated in Table 2. It should be mentioned here that the concentrations involved in Eq. (18) can be computed from the balance of the surface mass transfer rate with the product of the mass transfer coefficient and the concentration difference across the boundary layer. The mass transfer coefficient can readily be computed from the value of the Sherwood number obtained from Eq. (12).

It should be mentioned here that global reaction (16) is essentially dependent on the total concentration of the platinum catalyst layer. Therefore, the preexponential constant values reported in Table 2 reflect only implicitly such a dependence. This is because, in the present work, a fixed value is assigned to the total concentration of the active catalytic platinum surface sites. Equations (12) and (18) are needed to establish a simple model for the calculation of the heat and mass transfer rates in more complicated geometries, such as the catalytic reactors.

IV. Conclusions

The present paper describes a complete computational model for the prediction of the properties of reacting hydrogen–air mixtures impinging over hot catalytic surfaces. For a surface temperature of 1150 K, the impinging gas mixture reacts mainly on the surface with the active uncovered platinum sites, which represent about 99% of the catalytic surface area. The computed surface production rates of the flowing gas phase show consistency with the stoichiometric coefficients of the main reacting species in such a way that the consumption of H_2 by one-half moles of O_2 produces approximately 1 mole of H_2O. This shows that the production of rare species, such as OH and O, is not appreciable, although they may be the main factors affecting the global reaction rate as given by Eq. (13). New numerical correlations for the global reaction rate of H_2 with O_2 and the Sherwood number vs the Reynolds number were deduced for am Re ranging from 58 to 2315. As the Reynolds number increases, both the Sherwood number and the surface reaction rate increase almost linearly. On the other hand, the active boundary-layer thickness decreased from 1.0 to 0.25 cm as the inlet velocity increased from 15 to 150 cm/s due to the reduced transport against the approaching gas mixture toward the catalytic surface. The H atom and OH radical are produced on the surface, whereas the O atom is consumed by catalytic reactions. The present heat transfer numerical data can be correlated by equations similar to impinging nonreacting flows. However, a slightly higher dependence of the Nu on the Re is predicted for the impinging reacting flow. A new one-step, chemical kinetic surface reaction rate equation is numerically deduced, which is independent of the Re. This surface reaction rate equation is dependent on the reactant concentrations and the surface temperature. The new correlations can be used as a global heterogeneous surface reaction submodel for the more complicated 3-D catalytic combustors. The surface reaction rates of the stoichiometric hydrogen–air mixtures are nearly double that of its methane–air counterpart.

References

[1] Cattolica, R. J., and Schefer, R. W., "Effect of Surface Chemistry on the Development of the (OH) in a Combustion Boundary Layer," *19th Symposium (International) on Combustion*, The Combustion Institute, Pittsburgh, PA, 1982, pp. 311–318.

[2] Cattolica, R. J., and Schefer, R. W., "Laser Fluorescence Measurements of the OH Concentration in a Combustion Boundary Layer," *Combustion Science and Technology*, Vol. 30, Nos. 1–6, Jan. 1983, pp. 205–212. doi:10.1080/00102208308923620

[3] Ljungström, S., Kasemo, B., Rosen, A., Wahnström, T., and Fridell, E., "An Experimental Study of the Kinetics of OH and H_2O Formation on Pt in the $H_2 + O_2$ Reaction," *Surface Science*, Vol. 216, Nos. 1–2, 1989, pp. 63–92. doi:10.1016/0039-6028(89)90644-4

[4] Williams, W. R., Stenzel, M. T., Song, X., and Schmidt, L. D., "Bifurcation Behavior in Homogeneous-Heterogeneous Combustion: I. Experimental Results over Platinum," *Combustion and Flame*, Vol. 84, Nos. 3–4, 1991, pp. 277–291. doi:10.1016/0010-2180(91)90006-W

[5] Song, X., Williams, W. R., Schmidt, L. D., and Aris, R., "Bifurcation Behavior in Homogeneous-Heterogeneous Combustion: II. Computations for Stagnation-Point Flow," *Combustion and Flame*, Vol. 84, Nos. 3–4, 1991, pp. 292–311.
doi:10.1016/0010-2180(91)90007-X

[6] Warnatz, J., Allendorf, M. D., Kee, R. J., and Coltrin, M. E., "A Model of Elementary Chemistry and Fluid Mechanics in the Combustion of Hydrogen on Platinum Surfaces," *Combustion and Flame*, Vol. 96, No. 4, 1994, pp. 393–406.
doi:10.1016/0010-2180(94)90107-4

[7] Deutschmann, O., Behrendt, F., and Warnatz, J., "Modeling and Simulation of Heterogeneous Oxidation of Methane on a Platinum Foil," *Catalysis Today*, Vol. 21, Nos. 2–3, 1994, pp. 461–470.
doi:10.1016/0920-5861(94)80168-1

[8] Raja, L. L., Kee, R. J., Deutschmann, O., Warnatz, J., and Schmidt, L. D., "A Critical Evaluation of Navier-Stokes, Boundary-Layer, and Plug-Flow Models of the Flow and Chemistry in a Catalytic-Combustion Monolith," *Catalysis Today*, Vol. 59, Nos. 1–2, 2000, pp. 47–60.
doi:10.1016/S0920-5861(00)00271-6

[9] Tong, T. W., Abou-Ellail, M. M. M., and Li, Y., "Mathematical Modeling of Catalytic-Surface Combustion of Reacting Flows," *Journal of Thermophysics and Heat Transfer*, Vol. 21, No. 3, 2007, pp. 512–519.
doi:10.2514/1.27014

[10] Coltrin, M. E., Kee, R. J., and Rupley, F. M., "Surface Chemkin: A General Formalism and Software for Analyzing Heterogeneous Chemical Kinetics at a Gas-Surface Interface," *International Journal of Chemical Kinetics*, Vol. 23, No. 12, 1991, pp. 1111–1128.
doi:10.1002/kin.550231205

[11] Abou-Ellail, M. M., Gosman, A. D., Lockwood, F. C., and Megahed, I. E. A., "Description and Validation of a Three-Dimensional Procedure for Combustion Chamber Flows," *Journal of Energy*, Vol. 2, No. 2, 1978, pp. 71–80.
doi:10.2514/3.62365; also *Turbulent Combustion*, edited by L. A. Kennedy, Vol. 58, Progress in Astronautics and Aeronautics, AIAA, New York, 1978, pp. 163–190.

[12] Tong, T. W., Abou-Ellail, M. M., Li, Y., and Beshay, K. R., "Numerical Computation of Reacting Flow in Porous Burners with an Extended CH4–Air Reaction Mechanism," American Society of Mechanical Engineers Paper HT-FED 2004-56012, 2004.

[13] Peters, N., "Flame Calculations with Reduced Mechanisms," *Reduced Kinetic Mechanisms for Applications in Combustion Systems*, edited by N. Peters, and B, Rogg, Lecture Notes in Physics, Springer–Verlag, Berlin/New York/Heidelberg, 1993.

[14] Peters, N., "Laminar Diffusion Flamelet Models in Non-Premixed Turbulent Combustion," *Progress in Energy and Combustion Science*, Vol. 10, No. 3, 1984, pp. 319–339.
doi:10.1016/0360-1285(84)90114-X

[15] Kee, R. J., Rupley, F. M., and Miller, J. A., "The Chemkin Thermodynamic Data Base," Sandia National Laboratories Rept. SAND87-8215B, 1996.

[16] Deutschmann, O., Maier, L. I., Riedel, U., Stroemman, A. H., and Dibble, R. W., "Hydrogen Assisted Catalytic Combustion of Methane on Platinum," *Catalysis Today*, Vol. 59, Nos. 1–2, 2000, pp. 141–150.
doi:10.1016/S0920-5861(00)00279-0

[17] Tong, T. W., Abou-Ellail, M. M. M., and Li, Y., "Mathematical Modeling of Heat and Mass Transfer in Methane-Air Mixtures Flowing over Catalytic Surfaces," Begell House, Inc., Paper COM-09, 2006.

[18] Tong, T. W., Abou-Ellail, M. M. M., and Li, Y., "A Mathematical Model for Heat and Mass Transfer in Methane-air Boundary Layers with Catalytic Surface Reactions," *Journal of Heat Transfer*, Vol. 129, No. 8, 2007, pp. 939–950.
doi:10.1115/1.2737479

[19] Beitelmal, A. H., Shah, A. J., and Saad, M. A., "Analysis of an Impinging Two-Dimensional Jet," *Journal of Heat Transfer*, Vol. 128, No. 3, 2006, pp. 307–310.
doi:10.1115/1.2150841